Hybrid particle-fluid plasma modeling of Hall effect thrusters and analysis of non-conventional configurations

I. Fernández-Tena
Supervisors: J. Zhou, A. Domínguez-Vázquez & E. Ahedo

Equipo de Propulsión Espacial y Plasmas
Department of Aerospace Engineering, Universidad Carlos III de Madrid

Cylindrical Hall Thrusters (CHT)

- CHT **replaces** the conventional **annular chamber** of a traditional Hall effect thruster (HET) with a **cylindrical** one.
- This configuration **eliminates plasma losses** on the inner wall of the annular chamber and improves the efficiency of small, low-power prototypes.
- **Similar working principle** of a classical of a **HET** but notably with a more axial magnetic field (similar to a magnetic nozzle).
- **Prototype** developed at **EP2**.

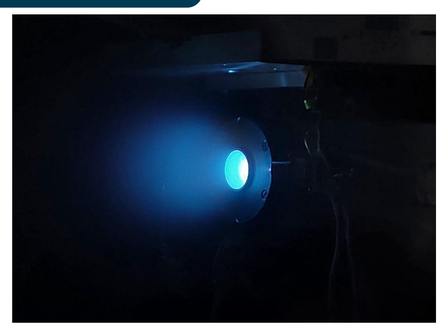

FIG. 1: Picture of the ignited CHT with xenon [1].

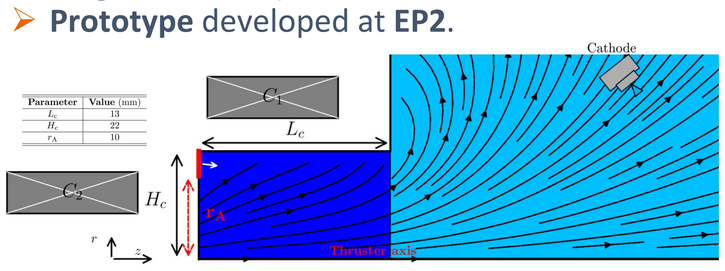

FIG. 2: Sketch of the CHT's chamber and near plume regions.

Neutrals are injected at the anode and ionized in the chamber. **Ions** are accelerated downstream by the anode-cathode potential. **Electrons**, injected at the cathode, ionize neutrals and neutralize the ion beam downstream.

PhD Motivation

This thesis seeks to advance the understanding of key design parameters in unconventional HET prototypes, focusing on low-power CHTs and high-power NHTs. Its objectives are organized into four main blocks:

- ❑ **State of the art and familiarization with HYPHEN.** Study and understand the main challenges associated with unconventional HET as well as the current situation of the HYPHEN simulation code [2].
- ❑ **Modeling of the CHT.** Numerical simulations of the CHT prototype developed by EP2 using HYPHEN to identify sources of inefficiencies and design parameters that enable optimal performance.
- ❑ **Development of HYPHEN-CM.** Implementation of a Cylindrical Mesh in HYPHEN to replace MFAM, enabling the simulation of complex geometries and magnetic topologies, such as NHTs.
- ❑ **Modeling of the NHT.** Numerical simulations of the NHT with HYPHEN-CM, analyzing magnetic topology effects on wall loads, erosion, and coupling mechanisms of cathode-anode in the near plume.

Nested Hall Thruster (NHT)

- **NHT = multiple coaxial annular channels** sharing a central cathode; same principle as single-channel HET.
- **Better high-power scaling** than single-channel HETs, which become too large for spacecraft [3].
- **Independent or joint operation** of channels allows **flexible thrust and power control** — ideal for deep space missions.
- **Proven with X2 (2×10 kW)** and **X3 (3-channel, 100 kW-class)** thrusters [3].

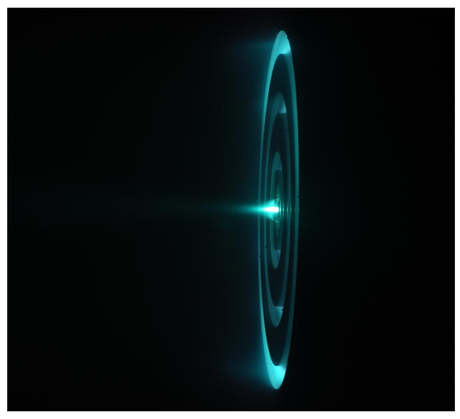

FIG. 3: Picture of the ignited X3 100-kW class NHT with xenon [3].

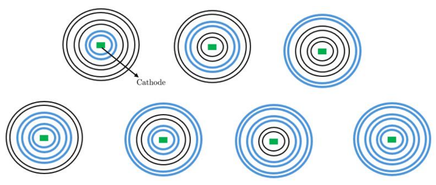

FIG. 4: Operation combinations of the X3 NHT channels.

HYPHEN-CM

- **HYPHEN** uses **three** main **modules**: **I-Module** for heavy species, **E-Module** for magnetized electrons and **S-Module** for the interaction of plasma bulk with the thruster walls. These modules are executed sequentially within a simulation loop.
- **I-module** operates on a structured **Cylindrical mesh**, **FIG. 5**, uses a **particle-in-cell (PIC)** method to solve the dynamics of ions and neutrals.
- **E-module** solves a quasineutral, drift-diffusion (inertialess) **fluid model** for the magnetized electron population, using a **MFAM**, **FIG. 6**.

HYPHEN-CM

Implementation of a **cylindrical mesh** for the E-Module:

- ✓ Avoid tedious meshing of the MFAM.
- ✓ Enable studies of complex magnetic topologies (NHT).

Issue to solve: numerical diffusion caused by strong magnetic anisotropy, which MFAM solved.

$$n_e = \sum_{s\neq e,n} Z_s n_s,$$

$$\nabla \cdot \boldsymbol{j}_e = -\nabla \cdot \boldsymbol{j}_i,$$

$$0 = -\nabla(n_e T_e) + e n_e \nabla\phi + \boldsymbol{j}_e \times \mathbf{B} + \mathbf{F}_{res} + \mathbf{F}_t.$$

$$\frac{\partial}{\partial t}\left(\frac{3}{2} n_e T_e\right) + \nabla \cdot \left(\frac{5}{2} n_e T_e \mathbf{u}_e + \mathbf{q}_e\right) = -\boldsymbol{j}_e \cdot \nabla\phi - Q_{inel},$$

$$\mathbf{q}_e = -\overline{\overline{K}}_e \cdot \nabla T_e.$$

$$\mathbf{F}_t \simeq -m_e \nu_t n_e u_{\theta e} \mathbf{1}_\theta, \quad \nu_t = \alpha_t \omega_{ce},$$

Preliminary Results of the Modeling of the CHT

Simulation Setup

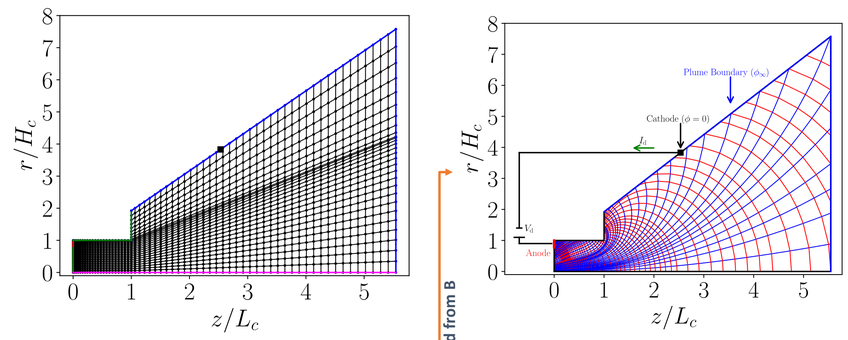

FIG. 5: The PIC mesh used to solve the I-module. Dielectric walls of the thruster, the symmetry axis, and the free-loss boundary are marked in green, magenta, and blue, respectively.

FIG. 6: The MFAM used to solve the E-module and the corresponding electric circuit. The cathode position is indicated with a black square. Inner blue and red lines represent parallel and perpendicular lines respect to the magnetic field, respectively.

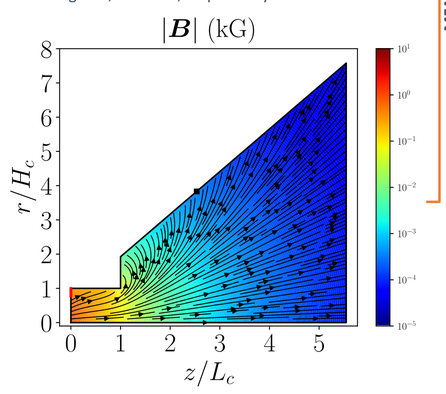

FIG. 7: 2D (z, r) contour plot of $|\mathbf{B}|$ in kG and its streamlines. The position of the anode is marked in red.

Simulation Parameters

Parameter	Units	Value
PIC mesh number of cells	#	1588
PIC mesh number of nodes	#	1683
PIC mesh smallest grid size	mm	0.75
MFAM number of cells	#	2248
MFAM number of faces	#	4569
MFAM average skewness	#	0.035
Ion-moving time step, Δt	ns	1.0
Initialization time steps	#	20000
Total time steps	#	60000
Total simulation time	μs	600
Injected Xe velocity	m/s	316
Injected Xe temperature	K	800
Injection Mach number	#	1.1

Considered Ionization Reactions

Reaction	ε_{th} (eV)
$e + Xe \rightarrow 2e + Xe^+$	12.13
$e + Xe \rightarrow 3e + Xe^{2+}$	21.21
$e + Xe \rightarrow 4e + Xe^{3+}$	32.06
$e + Xe^+ \rightarrow 2e + Xe^{2+}$	9.08
$e + Xe^+ \rightarrow 3e + Xe^{3+}$	19.93
$e + Xe^{2+} \rightarrow 2e + Xe^{3+}$	10.85

TAB. 1: Simulation parameters and considered ionization reactions.

Simulation Results & Comparison With Experiments

- **Four operational points (OPs)** has been simulated.

OP	V_d (V)	$\dot{m}_A$ (mg s^{-1})	Experimental I_d (A)	F (mN)	η_{thr} (%)	$\eta_u^{exp.}$ (%)	Simulation $(\alpha_{t1}, \alpha_{t2})$ (%)	I_d (A)	F (mN)	η_{thr} (%)	$\eta_u^{exp.}$ (%)
a	300	0.40	1.01	5.04	8.86	102	(5.40, 1.20)	1.02	5.12	8.76	97.0
b	300	0.45	1.06	5.96	10.5	110	(4.50, 1.00)	1.06	6.12	10.9	101
c	350	0.40	0.95	6.04	11.5	108	(4.50, 1.00)	1.00	6.22	11.3	99.0
d	350	0.45	1.09	6.89	11.9	112	(4.50, 0.93)	1.10	7.07	12.0	104

TAB. 2: The four considered OPs are defined by pairs of discharge voltage and anode mass flow. For each OP, experimental measurements [1] of discharge current, thrust, thrust efficiency and propellant utilization ($\eta_u^{exp} = \eta_u / \eta_{ch}$ "exp" indicates that the utilization is computed from the ion beam current, and η_{ch} denotes the charge efficiency) are available. In addition, the values of the turbulence parameters ($\alpha t1$, $\alpha t2$) used in the simulations are provided, selected to ensure that thrust efficiency matches the experimental value within a tolerance of 5%.

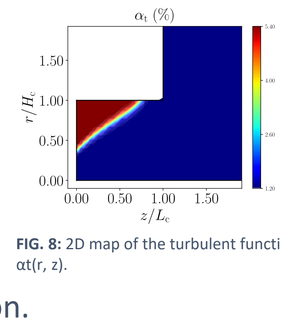

FIG. 8: 2D map of the turbulent function $\alpha t(r, z)$.

2D Maps.

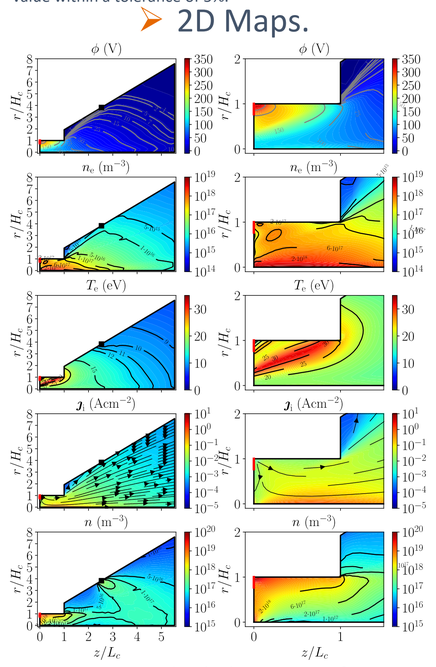

FIG. 8: Time-averaged 2D (z, r) contour maps for OP **a**, showing the full domain and chamber interior. From top to bottom: electric potential, plasma density, electron temperature, ion current, and neutral density.

Axial Profiles.

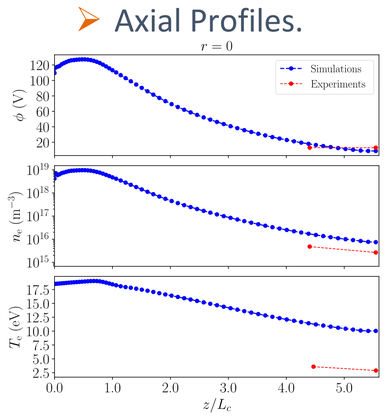

FIG. 9: Axial profiles at r=0 for OP **a**. From top to bottom: electric potential, plasma density and electron temperature.

Current Scan.

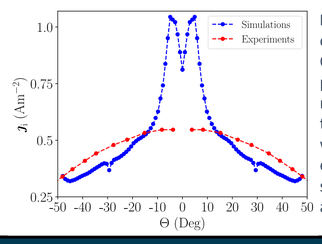

$$j_i = j_i \frac{r_{scan}}{r_{exp}}$$

FIG. 10: Angular scan of the ion current for OP **a**. Simulations are performed at a scan radius of 10 cm from the channel exit, whereas in the experiments the scan is conducted at a radius of 52 cm.

Ion Population.

Down 1 order of magnitude

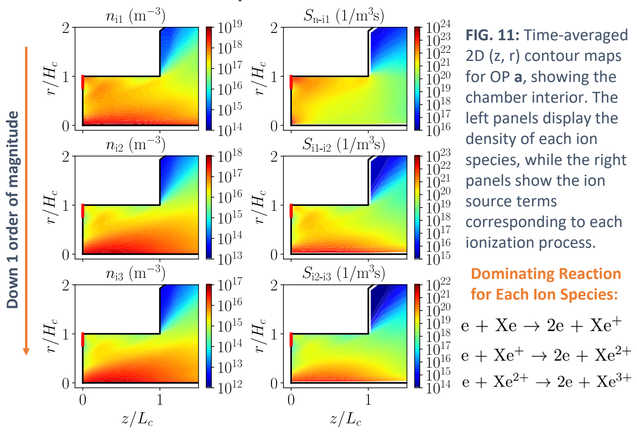

FIG. 11: Time-averaged 2D (z, r) contour maps for OP **a**, showing the chamber interior. The left panels display the density of each ion species, while the right panels show the ion source terms corresponding to each ionization process.

Dominating Reaction for Each Ion Species:

$e + Xe \rightarrow 2e + Xe^+$

$e + Xe^+ \rightarrow 2e + Xe^{2+}$

$e + Xe^{2+} \rightarrow 2e + Xe^{3+}$

Ion Energy Distribution Function.

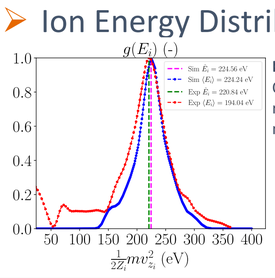

FIG. 12: Ion energy distribution function for OP **a**. For both simulation and experimental results, the most probable energy and the mean energy are indicated.

$$E_i = \frac{1}{2} m_i v_{zi}^2$$

$$g(E_i) = \frac{1}{\sqrt{2 m_i E_i}} \mathcal{F}_z\left(\sqrt{\frac{2E_i}{m_i}}\right)$$

Acknowledgments:

The author thanks Tatiana Perrotin, Prof. Jaume Navarro-Cavallé, and Dr. Jesús Perales-Díaz for their support on the development of the preliminary CHT results. This work was supported by the HEEP project, funded by the Agencia Estatal de Investigación under Grant Agreement No. PID2022-140035OB-I00.

References:

[1] - Tatiana Perrotin, Pablo Fajardo, and Jaume Navarro-Cavallé. Direct thrust measurements of a 200 w cylindrical hall thruster. In 38th International Electric Propulsion Conference, number IEPC-2024- 747, Toulouse, France, June 23-28, 2024. Electric Rocket Propulsion Society.

[2] - Domínguez Vázquez, A. (2019). Axisymmetric simulation codes for Hall effect thrusters and plasma plumes.

[3]- Hall, S. J., Cusson, S. E., & Gallimore, A. D. (2015). 30-kW Performance of a 100-kW Class Nested-channel Hall Thruster.

ep2@uc3m.es
https://ep2.uc3m.es